Joining Technologies: **Finite Element Modelling Of Electrode Wear Mechanisms**
(April 10, 1995)

Introduction

1.0 Introduction

Resistance spot welding is the principal joining method in auto body fabrication and assembly. In recent years, automobile designs have used an increasing amount of zinc-coated sheet steels. These steels are, in general, more difficult to weld than bare steels. The underlying mechanisms are not well understood. The zinc coating and changes in its thickness or composition are thought to play a role.

Galvanized steels have a thin layer of zinc which is applied to inhibit corrosion of the steel. During resistance welding, the zinc coating melts and some portion of the zinc alloys with the copper-based electrodes to form brass. The alloying process frequently causes non-uniform pitting of the electrode face as well as electrode edge degradation. In general, galvanized steels require higher welding currents and longer welding times than uncoated steels.

Galvanized steels also experience variations in weldability with increasing electrode wear. Generally, this is observed as a decrease in weld nugget size with an increasing number of welds. Interactions between the electrode face and the coating at high pressure and temperature conditions result in an increase in the electrode face diameter. This results in a decreased current density, decreasing the size of the weld formed. Electrode life is a major concern, as reported lives of zinc-coated steels are reported to range from a few hundred to a few thousand welds, while lives for uncoated steels range in the tens of thousands of welds.

Both hot-dipped galvanized (HDG) and electrogalvanized (EG) steels have been increasingly used to produce lighter weight and more corrosion-resistant vehicles. However, despite a number of advantages of the HDG over EG steels, it has been widely recognized that electrode lives for resistance spot welding of HDG steels are only about half those expected for EG steels. The explanation of this is not quite clear.

Analysis of electrode wear in resistance spot welding of coated steels is complicated by coupling effects of electrical, thermal, and mechanical interactions over the life span of an electrode. To gain a better understanding of the electrode wear mechanisms associated with resistance spot welding of HDG steels, the Auto/Steel Partnership has commissioned a number of research programs in recent years. In parallel with detailed metallurgical and weldability studies at Edison Welding Institute (EWI) and Michigan Technological University, Battelle was contracted to conduct a preliminary study on finite-element modeling of electrode wear mechanisms. The objectives of this finite-element modeling are as follows:

Develop appropriate finite-element modeling techniques for simulating the electric, thermal, and mechanical aspects of the resistance welding spot processes; in particular, those closely associated with electrode wear mechanisms.

Demonstrate the effectiveness of the finite-element modeling techniques in understanding electrode wear mechanisms by carrying out analyses for electrode face extrusion and pitting.

2.0 Finite Element Modeling

There has been a great deal of effort devoted to understanding the nugget formation in the open literature. Representative work along this line can be found in Gould (1987), Nied (1984), Tsai (1991), and others. In some of the recent work, finite element methods have been used in analyzing the process physics and mechanics associated with electric, thermal, and mechanical interactions during the nugget formation process. Some of the results obtained thus far prove to be extremely useful in understanding the mechanisms of weld nugget formation. However, using finite element methods to simulate electrode wear phenomenon has not been attempted in the open literature.

To ensure success, this work was carried out in three phases. At first, the electrical-thermal process associated

with nugget formation was studied; the temperature history generated was then used to simulate the thermal-mechanical process during nugget formation; and finally, both the understanding and data generated during the first two phases were used to carry out a preliminary analysis of electrode wear mechanisms.

2.1 Electrical-Thermal Simulation

A representative electrode design selected for analysis is illustrated in Figure 1. The corresponding 3-D finite element model is shown in Figure 2. Note that an angular sector of the electrode was modelled here to take advantage of the cyclic symmetry conditions with respect to cooling fins. The electric and thermal boundary conditions were properly imposed. The welding parameters were assumed as follows:

- Current (I) = 11,000 A (RMS)
- Squeeze force = 700 pounds
- Weld time = 12 cycles (0.2 sec).

Figure 3 shows the predicted temperature profile at the end of the welding cycle (Joule heating). The temperature range above 2,800 F (in red) presents the nugget size predicted. Note that temperature distribution surrounding the weld nugget was not influenced by the presence of the cooling fins, at least not at the early stage of the cooling process. It then follows that the 3-D finite element model with cooling fins is not necessary for studying the nugget formation process. This observation ensures the adequacy of using axisymmetric solid models from this point on, significantly reducing modelling complexities and computational requirements. The temperature history generated here was used for the thermomechanical simulation presented in the next section.

2.2 Thermal Mechanical Simulation

For computational efficiency, an axisymmetric finite element model was used for thermal-mechanical simulation of the nugget formation process during resistance spot welding. The finite element model is shown in Figure 4. Interface elements were used to model the mechanical interactions at the faying surface between the electrode face and workpiece. The temperature history obtained from Section 2.1 was mapped onto this axisymmetric model with standard interpolation/extrapolation procedures. Actual mechanical properties both for the electrode and metal sheet were adopted in this model.

Figure 5 shows the pressure (σ_{yy}) distributions after applying squeeze pressure. It can be seen that the pressure distribution is not uniform along the interface. Severe pressure concentration occurs near at corner edge of the electrode face. At the end of nugget formation, the corresponding temperature distribution is shown in Figure 6. The pink-colored region represents the weld nugget. The dashed lines represent the original position of the electrode/workpiece assembly. The corresponding pressure distribution is given in Figure 7. It is rather interesting to note that a gap was developed at the peripheral of the electrode/workpiece interface, and that as a result, the pressure concentration moved inward toward the center of the electrode, as indicated by the blue-colored region.

Figure 8 shows the residual stress (σ_{yy}) distribution both within the electrode and workpiece at room temperature, in which the electrode was not in contact with the work- piece. It can been seen that the faying surface of the workpiece was indented. The residual stress along the axial direction of the electrode (σ_{yy}) was tensile (pink-colored region) at the weld throat. The workpiece was distorted ("spring-back" as typically referred to in the auto industry) after welding. It should be also noted that residual stresses were also present with the electrode after welding.

2.3 Electrode Wear Modelling

In this preliminary study, the feasibility of using the finite element modelling techniques developed in the above to investigate electrode wear mechanisms was explored. The modelling focus here was on a better understanding of thermomechanical conditions associated with the development of electrode face extrusion during welding. Pitting effect was also investigated.

To take into account the effect of ß γ-brass layers, as observed in A/SP's ongoing study (Reference 1), the

axisymmetric solid model used in Section 2.2 was modified, as shown in Figure 9. The four thin layers of elements were assigned with a yield strength lower than that for the electrode. Since there is no detailed information available on their accurate stress-strain curves, it was assumed that the yield strength for these elements was one-half of the yield strength of the electrode, without losing generality. The temperature history from Section 2.1 was mapped onto this modified finite element model to carry out the thermomechanical analysis.

2.3.1 Electrode Deformation Mechanism During First Weld

Figure 10 shows the deformation characteristics at four different stages of the first welding cycle. At first, an equivalent squeeze force of 1,000 pounds was applied, and the resulting deformation was shown on the upper-left corner. The deformation was not noticeable. As the Joule heating started, the rapid thermal expansion of the area surrounding the weld nugget pushed the electrode upward. The resulting deformation at the end of the nugget formation was on the upper-right corner in solid lines. It is worth noting that given the lower yield strength of the electrode surface layer, the deformation was still rather uniform. During the cooling phase of the welding cycle, electrode face extrusion started to occur. The deformation at the end of cooling was shown on the lower-left corner. It can be seen that radial extrusion started to occur at the corner of the electrode face. After the electrode was removed from the workpiece, the deformation of the electrode changed little, as shown on the lower-right corner.

2.3.2 Accumulative Electrode Deformation Mechanism

To study some of the cumulative effects over a number of welds, the same analysis as in Section 2.3.1 was carried out over 15 welding cycles. At the beginning of each new weld, the stress and deformation conditions obtained from the previous one were carried over as the initial conditions. The results after 15 welds were summarized in Figure 11. The permanent plastic deformation on the electrode face accumulated rapidly, as the number of welds increased. It can be seen that the electrode face deformation predicted after the 15th weld (see Figure 11) had began to resemble the extrusion characteristics as shown in Figure 12, where the micrographs of the electrode corner were taken from Reference 1.

The plastic strain distribution after the 13th weld is shown in Figure 13. Permanent plastic deformation was shown by color contours except the dark blue color. It is interesting to note that in addition to the severe plastic strain accumulation near the corner of the electrode face, plastic strains also started to develop within the electrode material away from the electrode corner area at this stage. Figure 14 shows the material movement directions after the 13th weld. Away from the electrode face corner, material moved towards the faying surface in a uniform manner due to the squeeze pressure. Near the corner of the electrode face, the material moved with large magnitudes to form an extruded configuration.

A severely extruded electrode would inevitably alter the electrode displacement (or force) history, which often serves as sensing parameters for feedback control purposes. To shed some light on this, the electrode displacement histories for the first and 14th welds are shown in Figures 15 and 16. Note that in these two figures an artificial time scale from 0 to 1 second was used to apply the squeeze force and that the actual welding cycle started at

time = 1 second. The same scale was used in these figures. The displacement values were calculated with reference to the original electrode flank position when the electrode was in contact with the workpiece before the first welding cycle.

Figure 15 shows that as the squeeze force reached its peak value (1,000 pounds), the electrode displacement moved downward in a linear fashion. As the Joule-heating started, the electrode was pushed upward to its upper limit at about 0.3 second. As the nugget was cooled down rapidly by its surrounding structure, the electrode moved downward again, with its final value determined by the amount of indentation on the faying surface. As the electrode started wearing out, as indicated in Figure 11, the displacement-time signature was significantly altered, as demonstrated in Figure 16. In this figure, the electrode displacement as a function of time became drastically different from the one shown in Figure 15 for the first weld. This also demonstrates that finite element techniques, such as those used in this investigation, can be used to understand process parameters and their implications on the weld nugget formation and electrode wear conditions.

2.3.3 Electrical-Thermal Simulation of Electrode Pitting Effect

Effects of pitting are currently being investigated in Reference 1 with detailed experimentation and some advanced experimental techniques, such as thermal imaging. In the following, an exploratory study using the finite element techniques was attempted to shed some additional light on the experimental results obtained thus far.

For simplicity, a circumferential pitting was assumed on the electrode face. More detailed resolution was required due to the dimension of the pit geometry. Two axisymmetric models were generated for comparison purposes, as shown in Figure 17.

The current density distributions as predicted at t = 0.2 second are shown in Figure 18. Comparing the current density distribution near the pitting area, one can find that the presence of pitting significantly altered the current density distribution near the pitting area. With pitting, the current density near the pitting edge became rather high, in comparison with that without pitting (see Figure 18b). This is mainly due to the intimate contact effect at the outer edge of the pit. The corresponding temperature distributions are shown in Figure 19. It is interesting to note that although the temperature near the edge of the pit was raised quite a bit, the nugget shape was virtually not affected.

Figure 20 shows the comparison of the temperature histories at both the outer edge and inside the pit. The temperature was significantly higher at the outer edge than inside. This prediction was confirmed by thermography results obtained in Reference 1.

3.0 Concluding Remarks

Although this investigation was exploratory in nature, there have been a number of intriguing findings that offer a great deal of insight on electrode wear mechanisms as well as the resistance welding process itself. They are summarized as follows:

3.1 Resistance Spot Welding Process

In preparation for modelling of electrode wear mechanisms, this investigation has revealed the detailed thermomechanical interactions during the nugget formation process. The residual stresses and distortions in both the electrode and the workpiece were predicted. This information is still not available yet in the open literature. As far as resistance welding process physics and mechanics are concerned, the following findings are particularly worth noting:

- Cooling fins in the electrode had a negligible effect on the nugget formation and electrode face temperature at the early stage of a welding cycle.

- On one hand, high temperature due to electrical and thermal contact resistance at the electrode/sheet faying surface is a major driving force for electrode wear, on the other, the high interface temperature also serves as a thermal barrier that facilitates a proper nugget growth during welding. As a result, reducing the interface temperature below the melting temperature of zinc to prevent electrode wear seems not possible. The nugget will not form at all if the electrode/sheet interface temperature is lower than 900 F, based on the analysis carried out in this and a previous projects.

- The residual stresses at weld throat are highly tensile. Welding distortions (spring-back) can complicate the welding conditions in multi-weld sheet-metal structures. The amount of spring-back is controlled by the yield strength of the sheet metals.

3.2 Electrode Wear Mechanisms

Electrode face extrusion and pitting effect were investigated in this preliminary study. The following findings are particularly interesting:

- Although the presence of weaker (- and (-brass layers on the electrode face may undoubtedly play an important role in the electrode face extrusion, the thermomechanical interactions (e.g., Joule heating and cooling, electrode and sheet interactions) associated with resistance welding process have been the

driving force in this process.

- Thermoplastic strains are accumulated as the number of welds increases. Plastic strains of large magnitude rapidly develop, initially near the edge of the electrode face, and then gradually extend to the center area of the electrode face and inside the electrode.

- Based on this preliminary study, it is felt that (squeeze) force-time function during a welding cycle can be of particular importance in controlling the electrode face extrusion process.

- More favorable pressure distribution over the electrode face may be achieved through electrode design to improve the electrode wear resistance.

- Electrode pitting causes high current density distribution at outer edge of the pit. Consistent with thermography observations (Reference 1), the temperature at the outer edge is higher than inside the pit. Although the nugget formation process is not affected at the early stage of the pitting process, the outer edge of the pit, heated to a higher temperature, tends to develop plastic flow much more easily than without pits. As a result, pitting tends to accelerate the electrode face extrusion.

4.0 Concluding Remarks

The authors acknowledge the enthusiastic support from all members of the Electrode Wear Task Force of A/SP during the course of this study. Mr. T. Liang of Ohio State University provided assistance in some of the model generations, analysis, and post processing to P. Dong of Battelle during this investigation.

5.0 References

1. M. D. Gugel, C.L. White, M. Kimchi, and K. Picket: "Mechanisms of Electrode Wear During Resistance Spot Welding Hot-Dipped Galvanized Steel", A/SP Technical Report, Auto/Steel Partnership, March 25, 1994.

Figure 1. Electrode design.
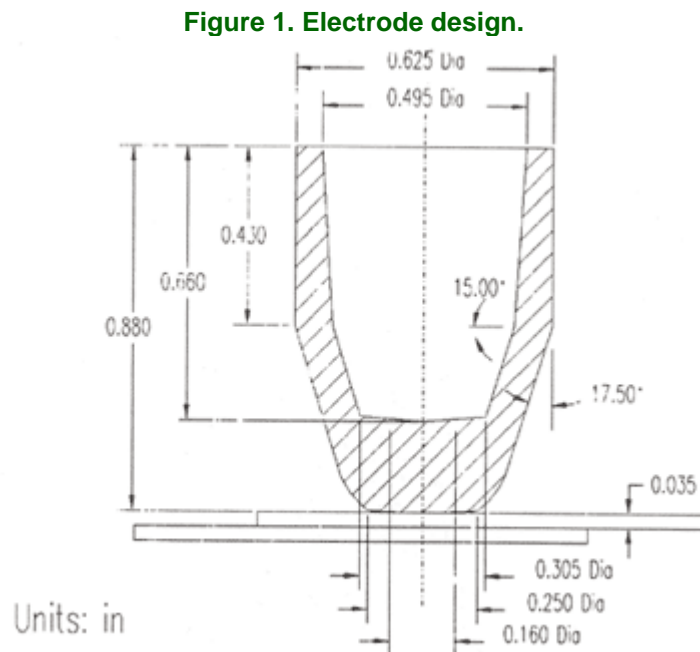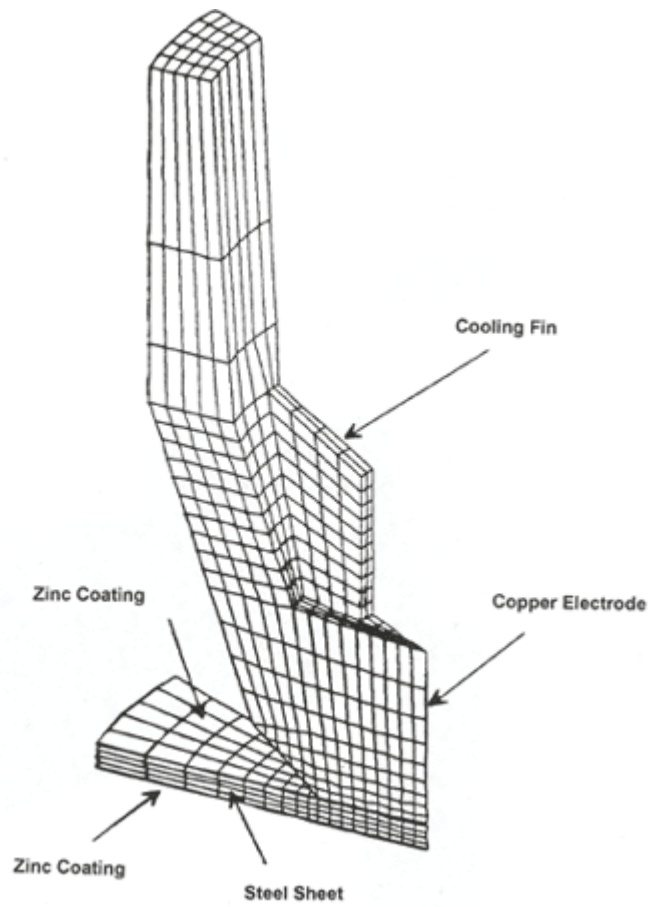

Figure 2. 3-D finite element model.

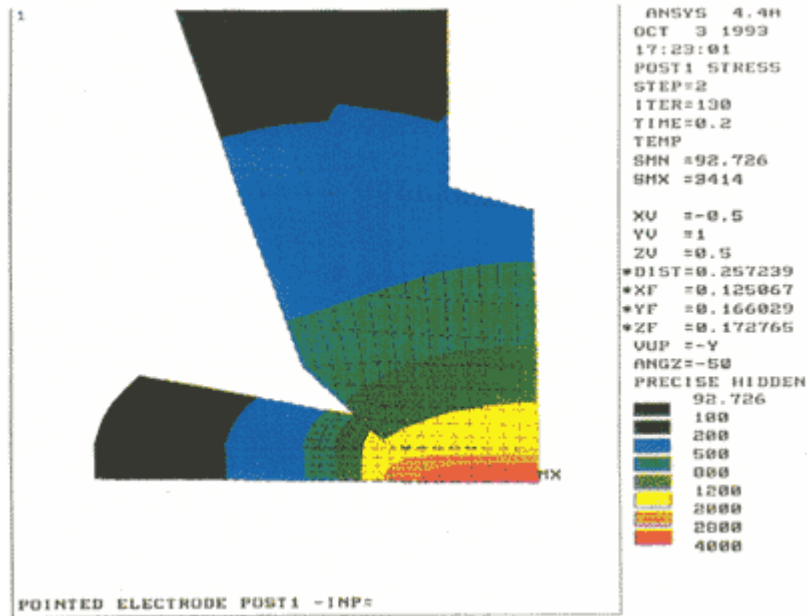**Figure 3. Nugget formal simulation.**

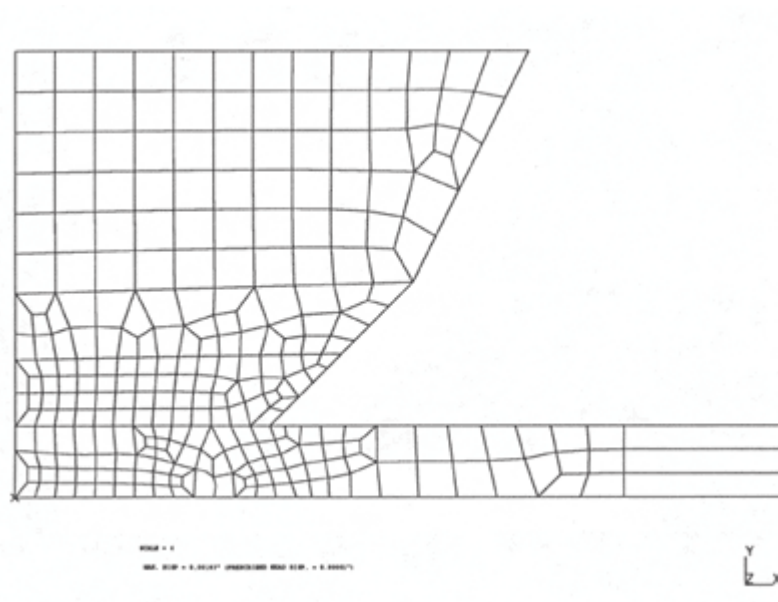**Figure 4. Simplified axisymmetric finite element model for thermo-mechanical simulation.**

Figure 5. Pressure (σ_{yy}) distribution after application of squeeze force.

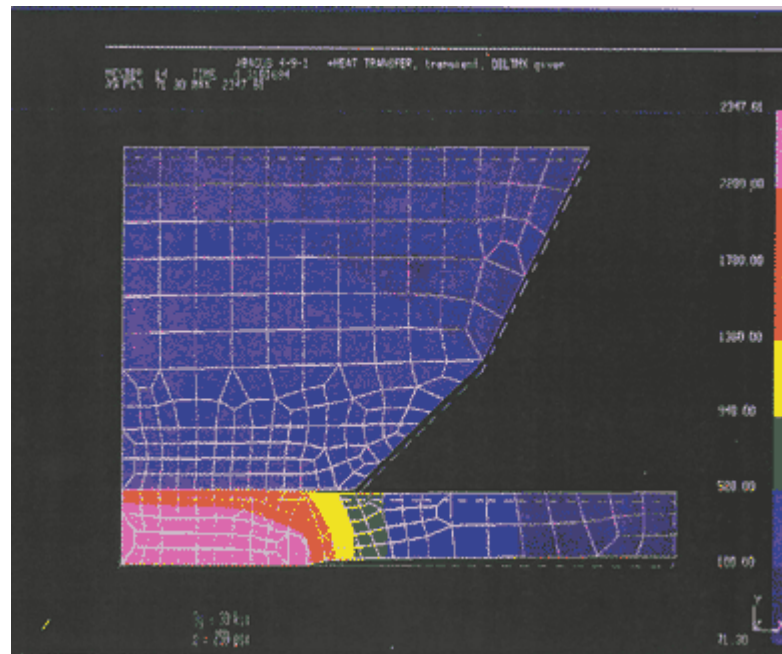**Figure 6. Temperature distribution at t = 0.31 seconds.**

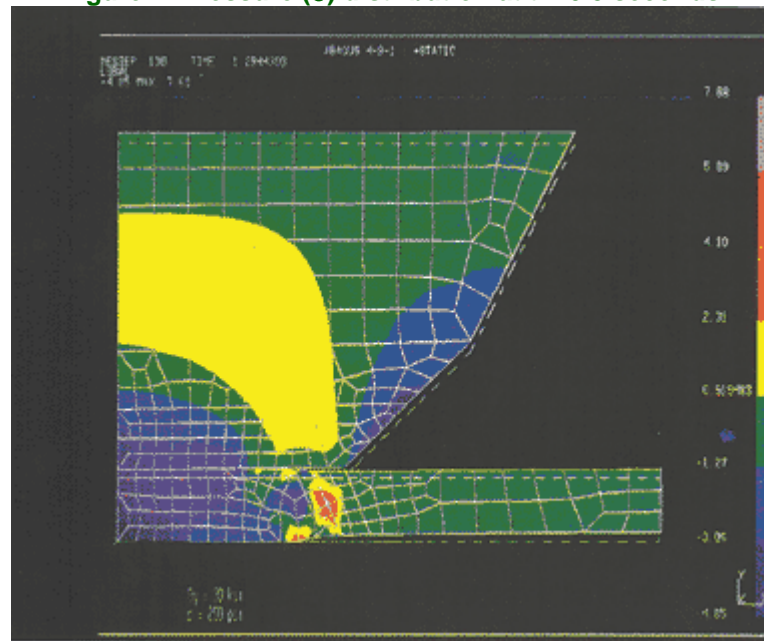Figure 7. Pressure (σ) distribution at t = 0.3 seconds.

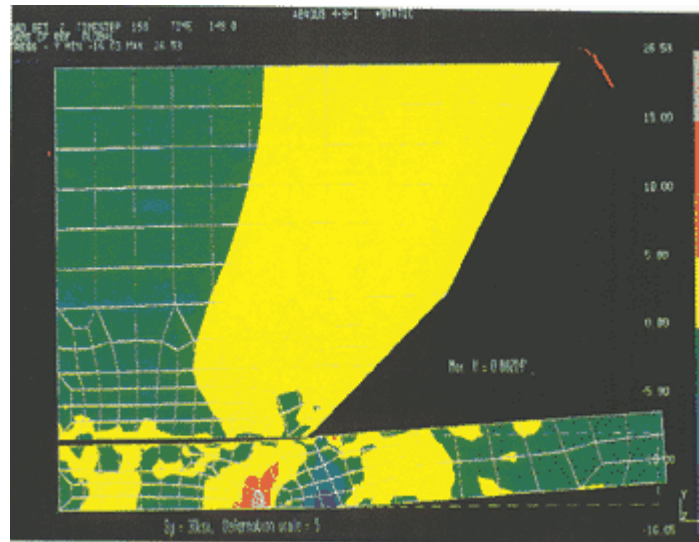Figure 8. Residual stress (σ) distribution at room temperature.

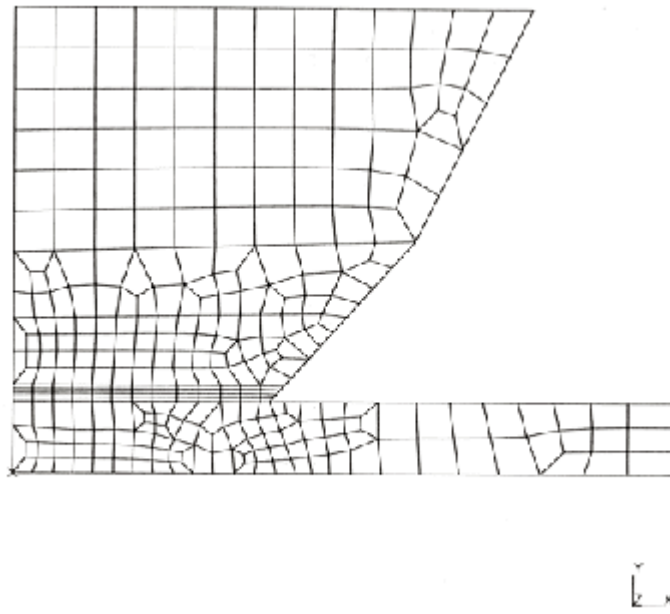**Figure 9. Modified axisymmetric solid element model (β
- and γ
-brass effects).**

**Figure 10. Deformation characteristics during the first weld (dashed lines = original shape; solid
lines = deformed shape).**
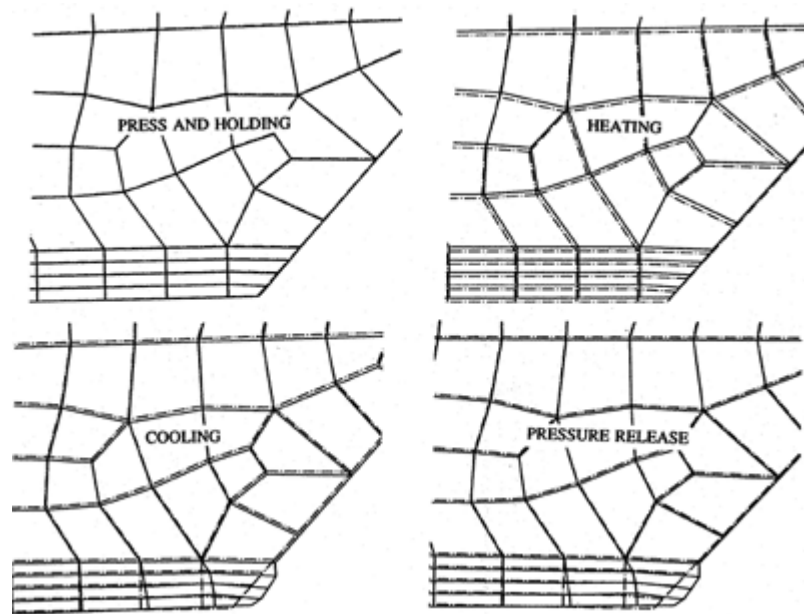
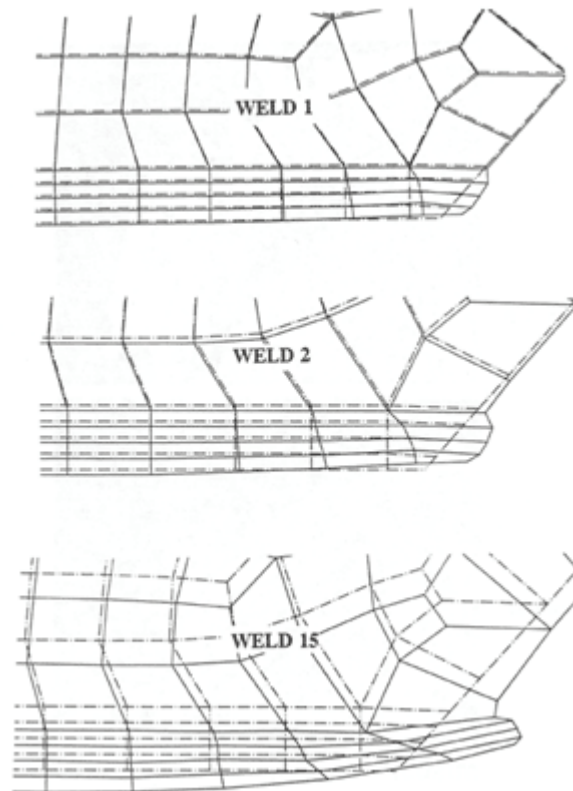**Figure 11. Deformation characteristics around electrode face: (a) After Weld 1, (b) After Weld 2, and (c) After Weld 15.**

Figure 12. Micrographs near the edge of an electrode tested on EG-1 to 2000 welds showing extrusion from electrode
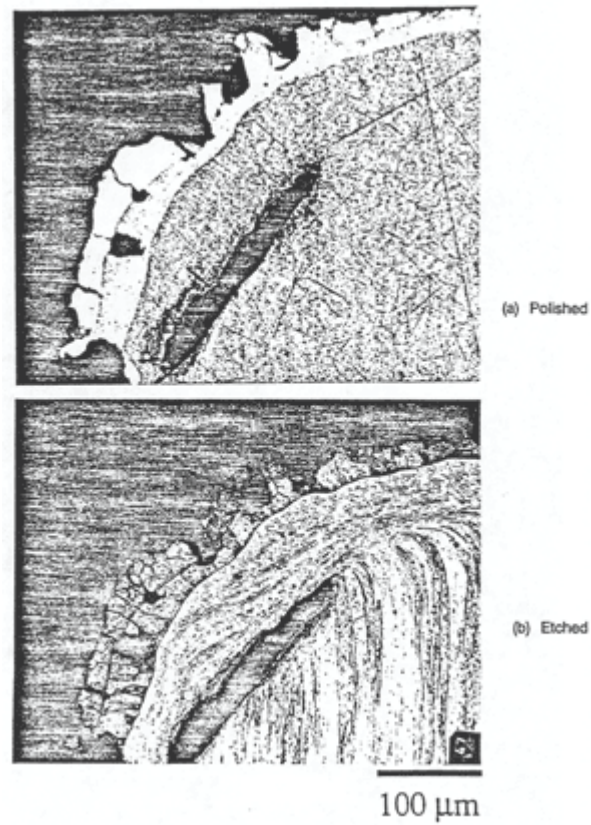
(a) Polished

(b) Etched

100 μm

Figure 13. Von Mises plastic strain accumulation at the electrode face after the 13th weld.
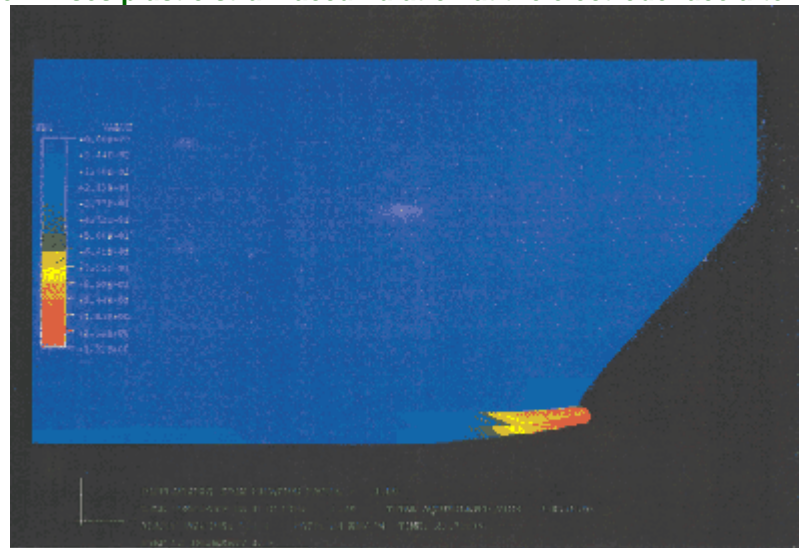

Figure 14. Material flow characteristics after the 13th weld (arrow direction = material flow directions; arrow sites = flow magnitudes).
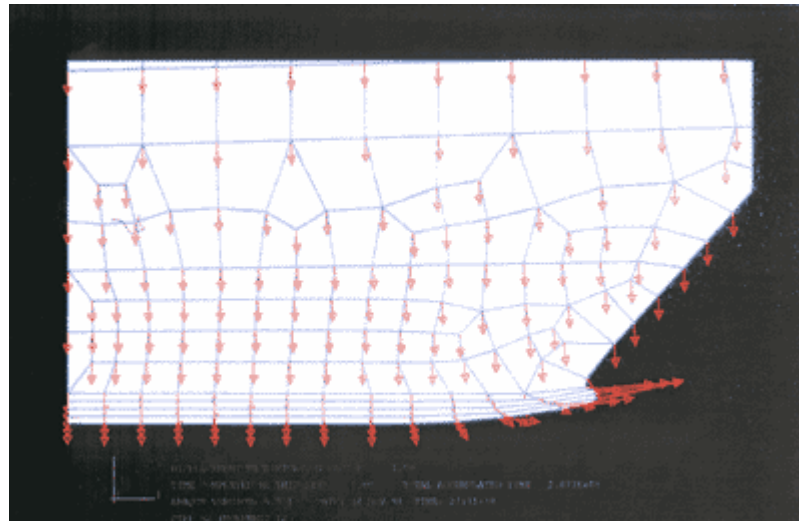
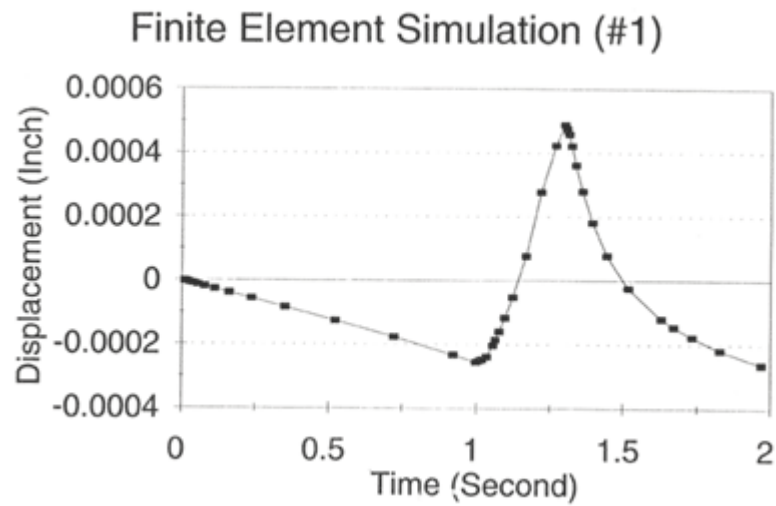**Figure 15. Predicted electrode displacement history after first weld.**

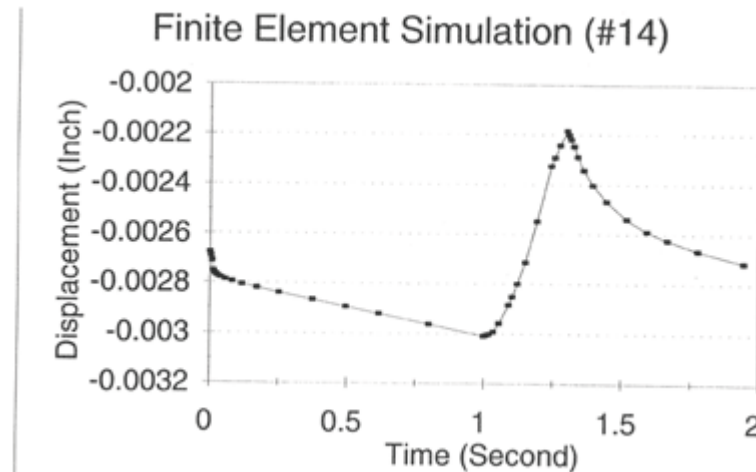**Figure 16. Predicted electrode displacement history after first weld.**

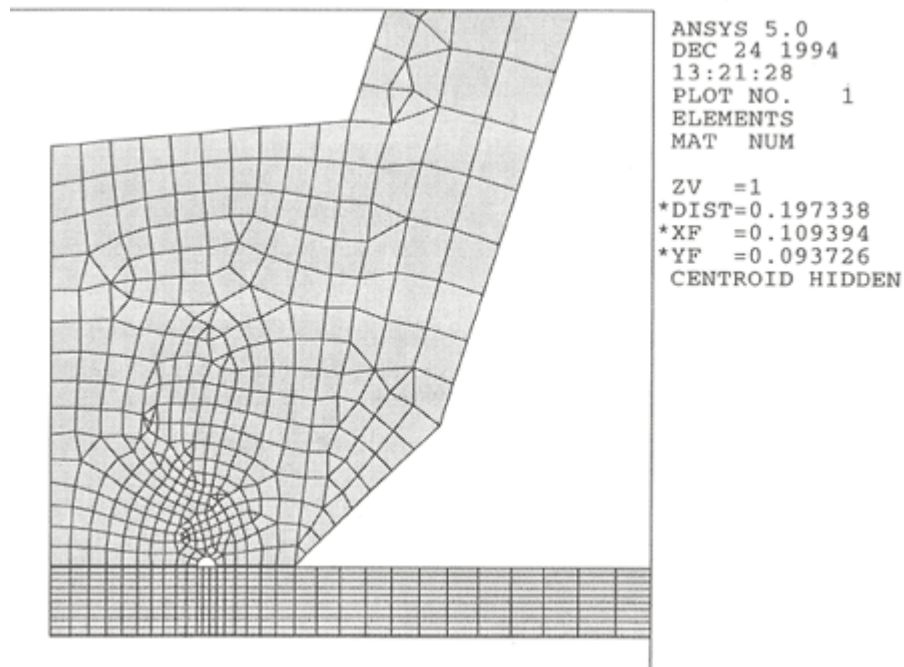**Figure 17a. FE models for pitting analysis: with a circumferential pit**

```
ANSYS 5.0
DEC 24 1994
13:21:28
PLOT NO.   1
ELEMENTS
MAT  NUM

ZV  =1
*DIST=0.197338
*XF  =0.109394
*YF  =0.093726
 CENTROID HIDDEN
```

Figure 17b. FE models for pitting analysis: without pitting


```
ANSYS 5.0
DEC 25 1994
10:45:31
PLOT NO.   1
ELEMENTS
MAT  NUM

ZV  =1
*DIST=0.148004
*XF  =0.101258
*YF  =0.056234
 CENTROID HIDDEN
```
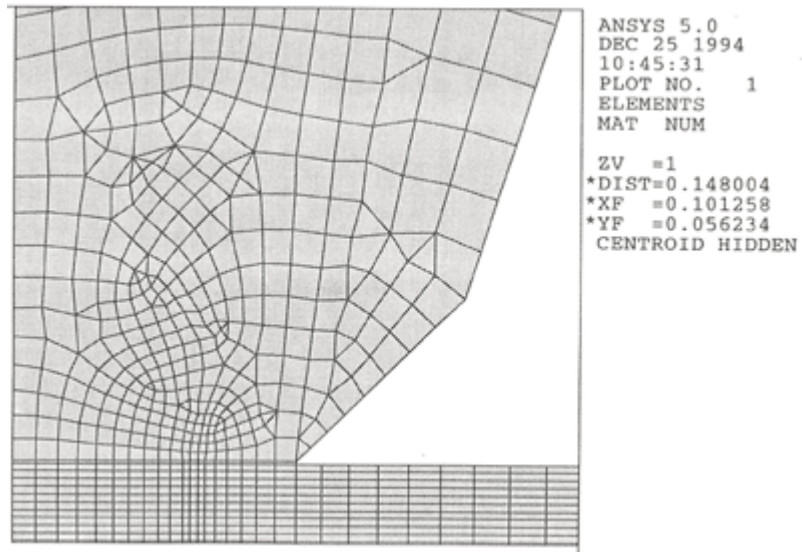
Figure 18a. Current density distributions at t = 0.2 seconds for electrodes with pitting.

ANSYS 5.0
DEC 26 1994
13:52:08
PLOT NO.   2
ELEMENT SOLUTION
STEP=1
SUB =53
TIME=0.2
JSY
SMN =-364.127
SMX =5.993
-440
-370
-300
-250
-200
-150
-100
-50
100
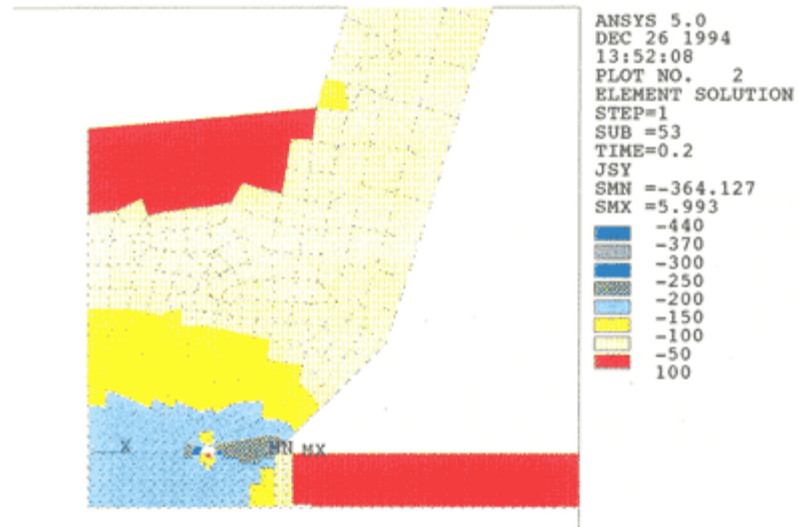
Figure 18b. Current density distributions at t = 0.2 seconds for electrodes without pitting.

ANSYS 5.0
DEC 26 1994
14:51:50
PLOT NO.   1
ELEMENT SOLUTION
STEP=1
SUB =49
TIME=0.2
JSY
SMN =-353.237
SMX =5.817
-353.237
-350
-300
-250
-200
-150
-100
-50
100
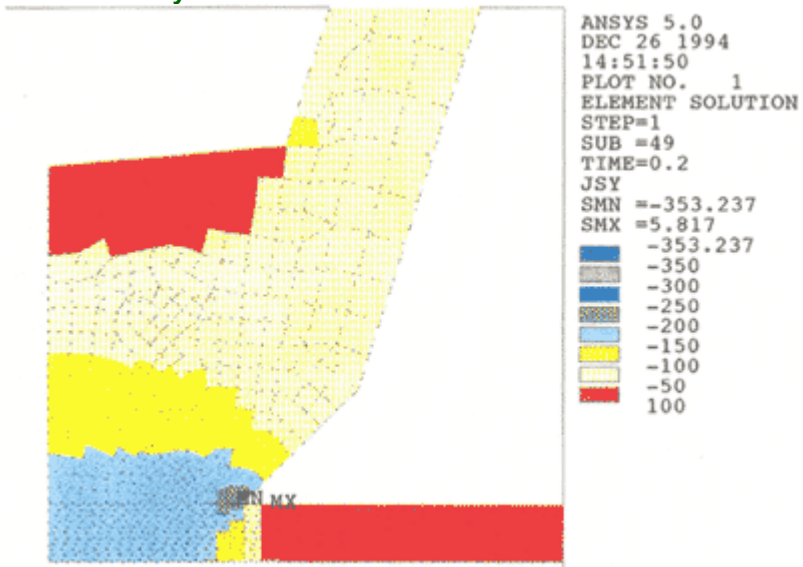
Figure 19a. Temperature distributions at t = 0.2 seconds with pitting.

```
ANSYS 5.0
DEC 26 1994
00:12:51
PLOT NO.    1
NODAL SOLUTION
STEP=1
SUB =53
TIME=0.2
TEMP
SMN =67.56
SMX =3660
       67.56
       1200
       1400
       1600
       1800
       2000
       2200
       2400
       4000
```

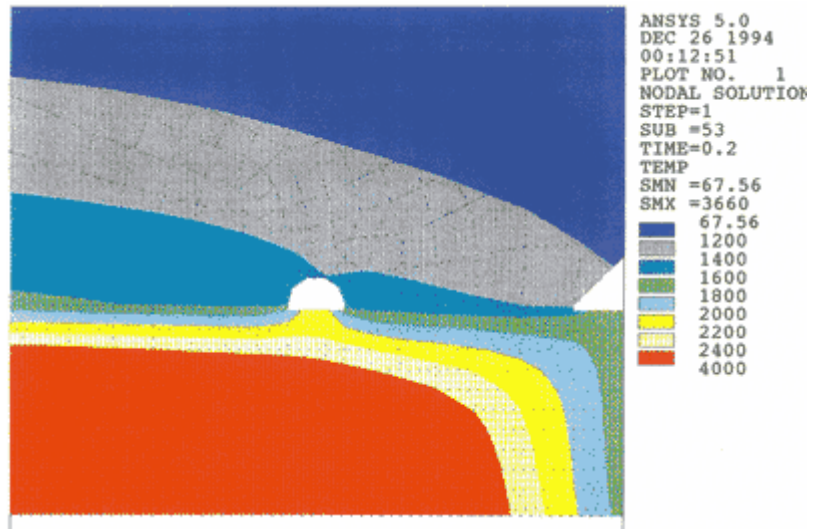**Figure 19b. Temperature distributions at t = 0.2 seconds without pitting.**


```
ANSYS 5.0
DEC 26 1994
14:42:46
PLOT NO.    1
NODAL SOLUTION
STEP=1
SUB =49
TIME=0.2
TEMP
TEPC=8.667
SMN =67.532
SMX =3565
       67.532
       1200
       1400
       1600
       1800
       2000
       2200
       2400
       4000
```